AIAA JOURNAL
Vol. 33, No. 11, November 1995

Experimental Study of Three-Dimensional Separation on a Large-Scale Model

D. Barberis* and P. Molton†
ONERA, 92322 Chatillon Cedex, France

Three-dimensional separation was studied by analyzing the flow past a large-scale model consisting of a half-prolate ellipsoid extended by a circular cylinder ending in a flat base at 45 deg with respect to the cylinder axis. The flow past the model, including boundary layer and vortical structures, was investigated in great detail using a three-component laser Doppler velocimetry system and three-hole pressure probes actuated by a displacement system installed inside the model. This last device allowed probing of the separating three-dimensional boundary layer very close to the surface. We observed how the boundary layer evolved as it gradually sheared into a vortex roll-up and then into an organized vortex. When skewing of the boundary layer increased, the difference in direction between the velocity gradient vector and the shear stress vector also increased. For this type of flow, turbulence models based on the assumption of isotropic turbulent viscosity are inadequate for numerical analysis.

Nomenclature

Cp	= static pressure coefficient
L	= model length
Re	= Reynolds number, $(V_0 L/\nu)$
V^i	= velocity components
V_e^i	= velocity components on the edge of the boundary layer
V_0	= upstream velocity at infinity
X^i	= coordinates of a point on the surface
α	= angle of attack of the model
ν	= kinematic viscosity
φ	= circumferential angle

Subscripts

$i = 1$ and 2	= components located in a plane parallel to the surface
$i = 3$	= component normal to the surface

Introduction

FLOW separation is a phenomenon of major importance for a large number of applications. Because it nearly always has detrimental effects, separation has been—and still is—the subject of many studies, both experimental and theoretical.

More precisely, the aim of this work was to study three-dimensional turbulent separation occurring on a regular surface whose radius of curvature was large compared with the thickness of the local boundary layer.

This problem has already been investigated in detail by focusing on a prolate spheroid with a 1:6 semiaxis ratio. One of the first authors to have studied the boundary layer developing on an ellipsoid of this shape set at an angle of attack was Eichelbrenner,[1] who proposed a three-dimensional laminar boundary-layer method. These calculations were validated by comparison with experiments carried out by Werle[2] in a water tunnel.

More recently, the experiments performed in air by Kreplin et al.[3,4] were extensively exploited. These experiments constituted several particularly well-documented test cases, including wall pressure and wall shear stress measurements as well as detailed flow probings with a multihole pressure probe. These experiments were conducted for two incidences: 10 and 30 deg. Results were obtained for both natural and forced transition; tests at high Reynolds numbers were made in a pressurized wind tunnel.[5,6]

These experiments were first used to validate boundary-layer calculations executed in the classical (or direct) mode, which consists in prescribing the outer velocity field.[7–13]

However, when separation occurs, some adjustment of the boundary-layer calculation was found to be necessary to avoid breakdown of the calculation in the immediate vicinity of separation. In this situation, the singularity in the boundary-layer equations can be circumvented by adopting an inverse mode in which either the displacement thicknesses or the skin-friction vector components are prescribed.[14–16] More recently, the prolate spheroid was used as a test case by the AGARD/FDP Working Group 10[17] created to investigate the limits of boundary-layer methods for calculation of three-dimensional turbulent separated flows.

Three-dimensional separation was also investigated on blunt obstacles other than the 1:6 prolate spheroid. The results obtained are specially interesting from a topological point of view with the description of the separation lines associated with the development of vortices for various model shapes.

At the end of the 1950s, experiments were performed on an oblate spheroid at an incidence.[18] Much later, Costis[19] and Costis et al.[20] investigated a laminar flow past a 1:4 prolate spheroid. These tests, which were carried out in a water tunnel, comprised flow visualizations and laser Doppler velocimetry (LDV) measurements. Barber and Simpson[21] published results obtained with a 1:6 prolate spheroid, significantly smaller than the model studied by Kreplin et al. They made their experiments for natural transition at an incidence of 10 deg. A five-hole pressure probe was used to define the mean velocity field in the vortex system and an X-wire probe to measure mean velocity and turbulent shear stress components in the boundary layer. Other important research, both experimental and theoretical, was conducted on the flow past a hemisphere cylinder set at an incidence.[22–24]

To conclude, Ramaprian et al.[25] reported results obtained on a model combining a hemispherical nose with a hemispheroidal rear part. These experiments included boundary-layer measurements with a three-hole pressure probe.

A preliminary approach to the three-dimensional separation problem can be made by studying the flow in a plane of symmetry. This situation is intermediate between a two-dimensional flow and a genuine three-dimensional situation. The boundary-layer equations are much simpler since the transverse velocity component V^2 is zero in a plane of symmetry; however, the problem still has a marked three-dimensional character, the transverse derivative of V^2 being different from zero. The magnitude of this derivative measures the degree of lateral convergence or divergence of the flow in the plane

Presented as AIAA Paper 93-3007 at the AIAA 24th Fluid Dynamics Conference, Orlando, FL, July 6–9, 1993; received March 2, 1994; revision received Feb. 8, 1995; accepted for publication Feb. 9, 1995.

*Head of Research Group, Aerodynamics Department, B.P. 72.
†Senior Technician, Aerodynamics Department, B.P. 72.

of symmetry. To our knowledge, the first author to have considered computation of a boundary layer in the plane of symmetry of a spheroid is Wang.[26] Other computations for the test case of Kreplin et al. were performed.[27–30]

Measurements in the plane of symmetry of the model combining a hemispherical nose with a hemispheroidal rear part were carried out by Patel and Baek.[31] These authors used their results in conjunction with a boundary-layer calculation employing the Cebeci–Smith turbulence model to study the effect of outer flow convergence or divergence on development of the boundary layer.[30] The theoretical prediction of this flow was improved by Sohn et al.[32] by introducing a modified (k, ε) turbulence model in the boundary-layer code.

A detailed experimental investigation of vortex formation was performed[33] on a model consisting of a half-oblate ellipsoid followed by a cylinder terminated by a slanted flat base. Surface flow visualizations were made in conjunction with field measurements by five-hole pressure probes and LDV techniques.

This paper reports on results obtained with an axisymmetric model tested in a subsonic wind tunnel. In this study, attention was focused on the boundary-layer evolution in the separation region and the mechanism leading to formation of a clearly detached primary vortex. The flow was investigated in detail using several experimental techniques: surface flow visualizations, surface pressure measurements, field explorations by multihole pressure probes, and an LDV system. The objectives of this investigation were to describe the boundary-layer behavior during three-dimensional separation and provide well-documented test cases to validate Navier–Stokes codes.

Experimental Conditions

Wind Tunnel and Model Definition

The tests were conducted in a closed circuit atmospheric wind tunnel driven by a fan with a constant blade angle and a variable speed motor with a maximum power of 700 kW. The test section is rectangular with a height of 1.8 m, a width of 1.4 m, and a length of 5 m (see Fig. 1). The airspeed can be varied from 10 to 100 m/s, and the stagnation pressure is equal to atmospheric pressure.[34] The shape of the model investigated was defined from preliminary tests executed in a water tunnel.[35] As shown in Fig. 1, the model consists of an axisymmetric half-prolate ellipsoid with a cylindrical extension terminated by a flat base, inclined at 45 deg with respect to the model axis, to stabilize separation on the rear part of the obstacle. The model length L from the nose to the middle of the base was equal to 1600 mm. The ellipsoid major axis $A1$ was 800 mm, and its minor axis $A3 = A2 = 200$ mm. The model incidence was adjusted via linkage. The horizontal sting was attached to a vertical mast crossing the test section. The vertical position of the sting was adjustable to be able to place the model in the center of the test section for different angles of attack.

Tests were carried out for an upstream velocity of 50 m/s and an incidence of 20 deg. All of the tests were conducted with natural transition.

Two models with the same shape were built. One was used for surface flow visualizations and LDV measurements and the other for surface pressure measurements and probing with a three-hole pressure probe. As shown in Fig. 2, the second model is in two parts.

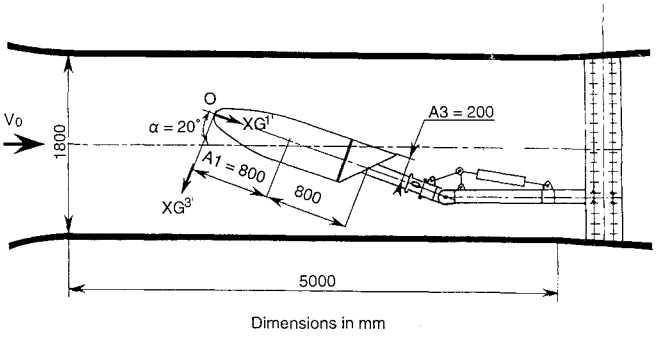

Fig. 1 Schematic representation of the model in the wind tunnel.

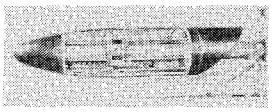

Fig. 2 View of the three-hole pressure probe displacement system installed inside the model.

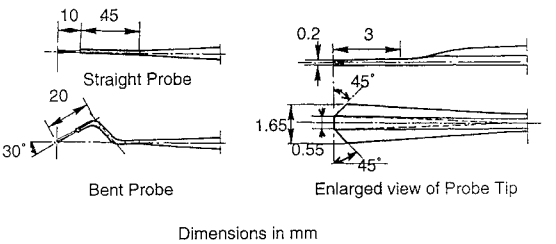

Fig. 3 Definition of the three-hole pressure probes.

The forward part, which can rotate along its longitudinal axis, contains a row of 46 surface pressure holes distributed along a meridian line. The traversing mechanism supporting the three-hole pressure probe is installed inside this forward part. It can be set to any longitudinal position in the range of 340 mm $< XG^{1'} <$ 900 mm ($XG^{1'}$ denotes the distance along the model longitudinal axis measured from the nose, as shown in Fig. 1). For the forward part, the traversing mechanism can rotate in such a way that the probe displacement remains normal to the surface at the measuring station (see Fig. 2).

The rear part of the model, with the flat base, is attached to the sting holding the model in the test section.

The traversing mechanism can be accessed through a large aperture in the model that is closed during operation (see Fig. 2).

Means of Investigation

For this study two types of investigation procedures were used. First, oil flow visualizations and surface pressure measurements were carried out to determine the flow structure on the wall. Second, the flowfield organization was defined using three-hole pressure probes and LDV.

The two three-hole pressure probes used to investigate the boundary layer are shown in Fig. 3. The minimum thickness of these probes is 0.2 mm and their width is 1.6 mm. Initial explorations were made with the straight probe. Then, in regions where the angle between the probe axis and the velocity vector was too high (>30 deg), the bent probe was used.

By proper calibration, three-hole pressure probes allow determination of the local stagnation pressure and local velocity vector (direction and magnitude). However, this determination is based on a boundary-layer type assumption that considers the velocity component normal to the surface to be negligible. Therefore, three-hole probes can only be used in regions without vortices, which would induce a normal velocity component. Some tests were conducted to qualify the effects of incidence and Reynolds number on the probe calibration curves.[36] These effects were found to be negligible for the range of parameters considered. A special study was also conducted to determine the wall effects on the probe readings. It was found that corrections were unnecessary when the distance to the wall exceeded the probe thickness (0.2 mm in our case).[37]

To avoid possible disturbances due to the presence of the probe in a region of vortex formation and also to determine the Reynolds tensor components, measurements were made using a three-component LDV system.

A schematic representation of the LDV system installed in the wind tunnel is shown in Fig. 4. This is a three-component system that can work in both the forward scatter and the backscatter modes of operation. The sources are two identical argon lasers with a maximum power of 15 W. The first laser produces the green ($\lambda = 0.5145$ μm) and blue ($\lambda = 0.488$ μm) emissions, the second giving the violet ($\lambda = 0.4765$ μm) component. The three pairs of beams resulting from crossing beam splitters are focused to form the probe volume whose useful diameter is 0.35 mm. The fringe spacing, which is the same for the three fringe patterns, is equal to 15 μm.

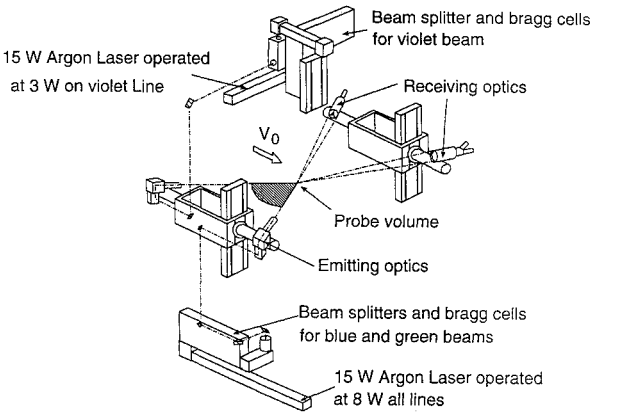

Fig. 4 General optical and mechanical disposal of the three component LDV system (forward mode).

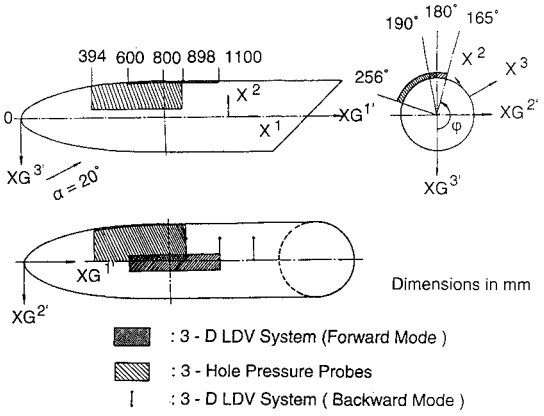

Fig. 5 Domains investigated: field measurements.

The directions of emission of the three colors are contained in the same horizontal plane (see Fig. 4), the angle between the violet beams and the green + blue beams being equal to 55.2 deg. The system was equipped with Bragg cells to determine the direction of the measured velocity component.

The scattered light was collected by two Cassegrain telescopes and applied to three photomultipliers (one for each component). The signals were processed by three DISA 55L counters. A dedicated on-line computer was used for control of the complete system and calculation of the statistical quantities (mean velocity and Reynolds tensor components).

The flow was seeded with incense smoke injected downstream of the test section, so as not to disturb the upstream flow by the injection device. To obtain the best signal-to-noise ratio, the system was operated in forward scatter mode. In this mode, the collecting optics are opposite the emitting part relative to the model. A good wall approach can only be achieved in the plane of symmetry of the model or its neighborhood. The backscatter mode of operation was used for measurements outside the plane of symmetry, on the side of the model. The collecting optics are then on the same side of the flow as the emitting part. With backscattering, the light scattered by the particles is 100–1000 times less intense than in forward scatter mode, causing a significant degrading of the signal-to-noise ratio. Furthermore, the light reflected by the surface when the laser beams strike the model tends to dazzle the collecting optics, which prevents measurements close to the surface. For this reason, the backscatter mode was used only in the three most downstream planes, where the vortex coming from separation is well detached from the surface.

Domains Investigated

Different domains were considered with respect to the physical phenomenon and the means of investigation.

Forty-six pressure taps were installed along the same meridian line between $XG^{1'} = 340$ and 1150 mm. The detailed pressure distributions were obtained by rotating the model around its roll axis, with a step of 1 deg.

The domains considered for field measurements are shown in Fig. 5. Since it is not possible to determine the normal velocity component directly, with three-hole pressure probes their use was restricted to the study of the boundary layer at the very first stage of the vortex development.

Accuracy

The upstream flow velocity accuracy was estimated with a relative error $\Delta V_0/V_0 = 1\%$. Accuracy of the geometrical incidence was equal to 0.02 deg. The uncertainty on surface pressure was $\Delta p = \pm 7$ Pa leading to an accuracy ΔKp of $\pm 1\%$ for $Kp = -0.5$.

For three-hole pressure probe measurements, the uncertainty on pressure measurements on each hole was ± 7 Pa, leading to an uncertainty of ± 0.4 deg on measurement of the direction of the velocity vector. The accuracy of the LDV measurements was estimated as ± 1 m/s for the value of the velocity and of ± 1 deg for the direction of the local velocity vector.

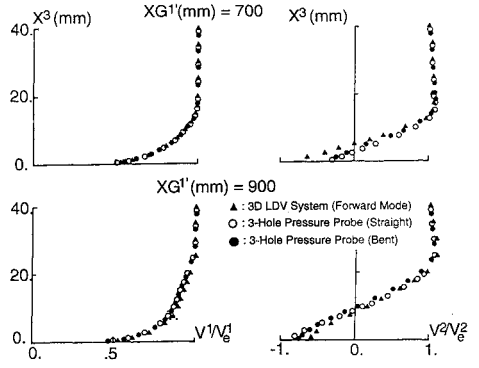

Fig. 6 Comparison between LDV and three-hole probe measurements. $\varphi = 170$ deg, $\alpha = 20$ deg, $V_0 = 50$ m/s, $R_e = 5.6 \times 10^6$.

Measurement Comparisons

Figure 5 shows that part of the domain investigated with the three-component LDV system in the forward mode was common with the one investigated with three-hole pressure probes. Furthermore, two three-hole pressure probes were used. Figure 6 shows a comparison between LDV and three-hole pressure probe measurements on the mean velocity components for the boundary layer in two locations. For the first station situated at $XG^{1'} = 700$ mm and $\varphi = 170$ deg, the agreement is good for the longitudinal component. For the transverse component we can see that the three means of investigations give the same results outside the boundary layer. Near the wall, LDV gave values lower than the pressure probes. The second station, situated at $XG^{1'} = 900$ mm and $\varphi = 170$ deg, corresponds to the beginning of the vortex. As in the previous section, the agreement is good for the mean longitudinal component. However, for the transverse component, LDV results gave an overestimated value of V^2 by comparison with the three-hole pressure probe. Two reasons can explain the discrepancies on the LDV results. The first is relative to the LDV procedure. An incense smoke injection device located downstream of the test section to avoid disturbing the incoming flow does not allow a high particle rate for measurements near the model surface. The second reason is relative to the location of the probe volume, which was very close to the wall, where large velocity gradients exist. Furthermore, near the wall, a difference appears between the bent probe and the straight probe. For the straight probe, the angle between the flow direction and the probe is large (>25 deg), whereas for the bent probe it is around zero. In this case, the indications of the bent probe are better than those of the straight probe.

Presentation of Results

Surface Flow Visualizations

Analysis of the surface flow was made using a mixture of paraffin oil, titanium dioxide, and oleic acid.

Figure 7 presents side and leeward views of the surface flow pattern obtained for $\alpha = 20$ deg. Near the model nose, local separation can be observed as an accumulation of the visualization product.

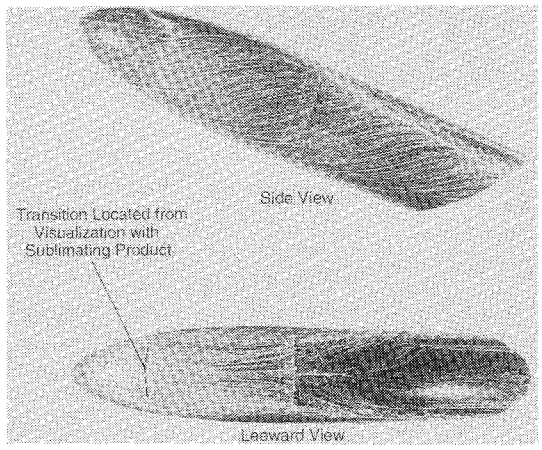

Fig. 7 Oil flow visualization. $\alpha = 20$ deg, $V_0 = 50$ m/s, $R_e = 5.6 \times 10^6$.

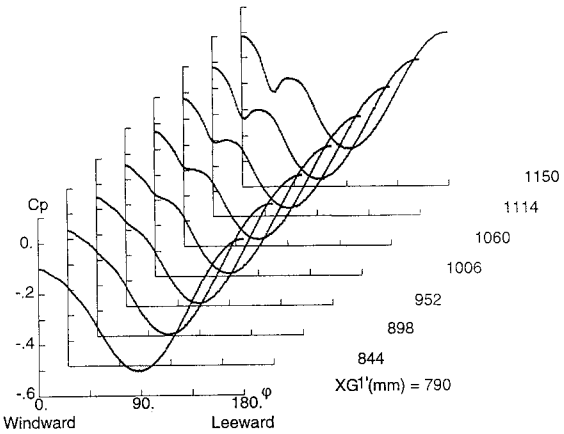

Fig. 8 Wall pressure distributions at various cross-sections. Model rear part. $\alpha = 20$ deg, $V_0 = 50$ m/s, $R_e = 5.6 \times 10^6$.

This separation caused a sudden transition of the flow from a laminar to turbulent state. This phenomenon was confirmed by visualizations made with a sublimating product.[38] This technique used the well-known property of acenaphthene to sublimate in the turbulent zone. The remaining acenaphthene then reveals the laminar region. On the rear part of the model, the skin-friction lines from the windward plane of symmetry converge towards a first separation line. A second separation line is present closer to the leeward plane of symmetry. The skin-friction lines on one side of this separation line come from the leeward plane of symmetry. The picture should be completed by three attachment lines: two in the windward and leeward planes of symmetry and one between the two separation lines.

Surface Pressure Distributions

The possibility of rotating the model around its roll axis allowed us to make extremely detailed surface pressure measurements along circumferential directions.[38] The rotation step for these measurements was equal to 1 deg, the circumferential lines being spaced 18 mm apart. Figure 8 shows the pressure distributions obtained at a 20-deg incidence.

The variation of the pressure distributions from one section to another is moderate. The maximum negative pressure peak occurred at 90 deg from the windward plane of symmetry, and then the pressure increased steadily up to the leeward side. However, for the last sections a small increase in the negative peak magnitude was observed just before the leeward plane of symmetry. Comparison between oil flow visualization and surface pressure measurements showed that for this incidence separation did not produce any substantial fluctuation of the surface pressure measurements.

Flowfield Measurements with the Three-Hole Pressure Probes

During the exploration procedure, the probe was displaced normal to the wall. The plane defined by the three holes of the probe was parallel to the wall. Thus, only the velocity components contained in a plane parallel to the local plane tangent to the surface were determined directly.

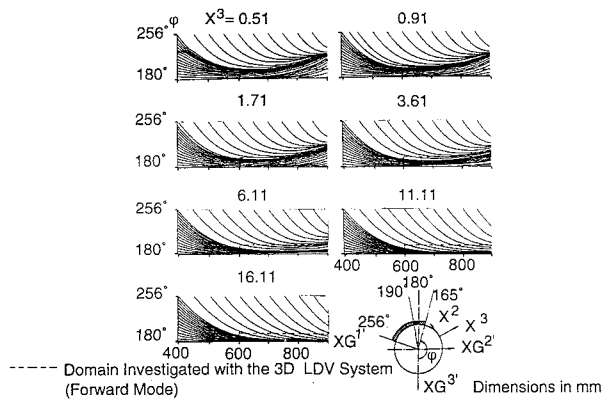

Fig. 9 Streamlines obtained from three hole pressure probe measurements. $\alpha = 20$ deg, $V_0 = 50$ m/s, $R_e = 5.6 \times 10^6$.

Figure 9 shows the streamlines of this vector field measured in portions of surface parallel to the obstacle surface and located at different heights. For the surfaces located at $X^3 = 11.11$ and 16.11 mm from the obstacle wall, the entire flow streams from the windward to the leeward side.

When approaching the obstacle, part of the flow coming from the leeward side tends towards a common direction defined by the convergence of the streamlines. At the distance $X^3 = 6.11$ mm, the line of convergence is located in the plane of symmetry, the flow being almost parallel to this plane.

For surfaces below $X^3 = 6.11$ mm, the convergence line leaves the plane of symmetry. Its distance from this plane increases in exploration surfaces even closer to the model wall.

For the surface located at $X^3 = 0.51$ mm, the closest to the model, local convergence of the streamlines is observed for the roll position $\varphi = 225$ deg and the longitudinal abscissa $XG^{1'} = 400$ mm. This convergence corresponds to the laminar separation region mentioned earlier. A convergence line exists between this region and the end of the investigated domain. This line can also be observed on the oil flow visualizations shown in Fig. 7 where it appears as a local accumulation of visualization product.

Comparisons between the surface located at $X^3 = 0.51$ mm and that located at $X^3 = 16.11$ mm allow an evaluation of skewing of the boundary layer. At $XG^{1'} = 900$ mm, skewing reaches a value of 60 deg.

As already mentioned, measurements with a three-hole pressure probe have several restrictions: they give no information on the velocity component normal to the model surface or on turbulent quantities. Furthermore, indications very close to the wall are perturbed by a probe displacement effect.

Boundary-Layer Measurements in the Vicinity of the Leeward Plane of Symmetry with the Three-Component LDV System

For these measurements, the LDV system was operated in forward scatter mode to give better access to the flow in the near-wall region. The investigated domain is shown in Figs. 5 and 9. Eleven cross sections were explored between $XG^{1'} = 600$ and 1100 mm, each containing five exploration lines normal to the model wall.

Figure 10 shows the projections of the mean velocity vector in planes normal to the longitudinal axis of the model. The origin of boundary-layer shearing in the upstream part of the domain explored is confined to the immediate vicinity of the surface and is thus inaccessible to LDV. Further downstream, vortex development can be observed as the vortex gradually detaches from the surface of the obstacle. The dashed line indicates the boundary between the part of the flow "leaving" the surface and the one "diving" towards the surface.

In Fig. 11 are compared the crosswise variations of the longitudinal mean velocity component V^1 in some of the explored sections. For the section at $XG^{1'} = 650$ mm, the velocity profiles are similar

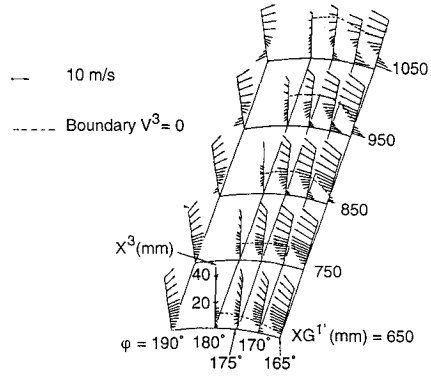

Fig. 10 Projections of the mean velocity vector in the planes normal to the longitudinal axis of the model. α = 20 deg, V_0 = 50 m/s, R_e = 5.6 × 10^6.

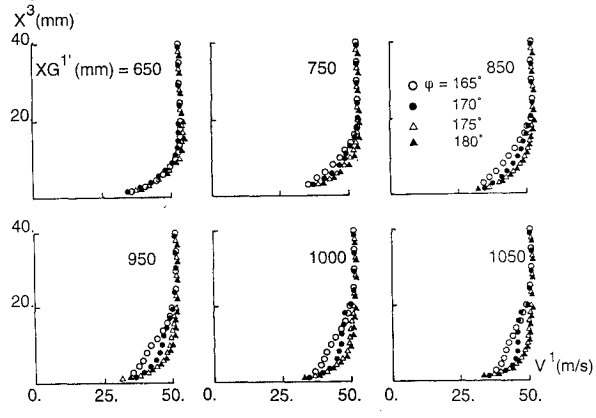

Fig. 11 Longitudinal mean velocity component V^1. α = 20 deg, V_0 = 50 m/s, R_e = 5.6 × 10^6.

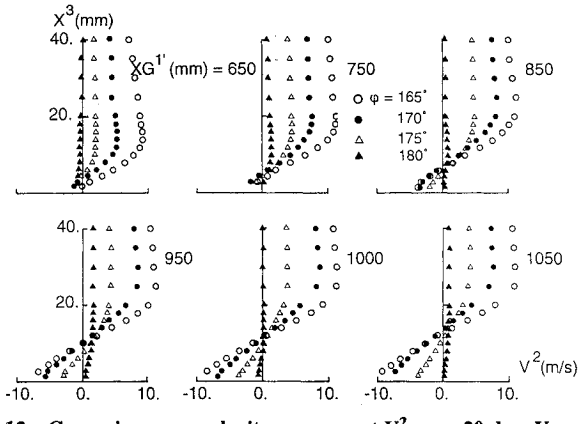

Fig. 12 Crosswise mean velocity component V^2. α = 20 deg, V_0 = 50 m/s, R_e = 5.6 × 10^6.

in appearance. For the other sections, the profile shapes along the meridian lines φ = 180 and 175 deg are roughly the same; however, the variations for the other φ lines are characterized by the existence of an inflection point.

The profiles of the crosswise mean velocity component V^2 are plotted in Fig. 12. This component should be zero in the vertical plane of symmetry. However, nonzero values are observed in some sections due to measurement uncertainties. The maximum value of V^2 is less than 2 m/s, which corresponds approximately to $0.04V^1_{\text{ext}}$ (value of the longitudinal component at the boundary-layer edge).

By comparison with the longitudinal component V^1, the crosswise component V^2 varies more slowly. Except for the results in the plane of symmetry, each profile exhibits two well-defined portions: an outer part where the flow converges towards the plane of symmetry and an inner part where it diverges from this plane. This inner part of the profiles grows in size in the sections farthest downstream. In addition, the point where the flow is parallel

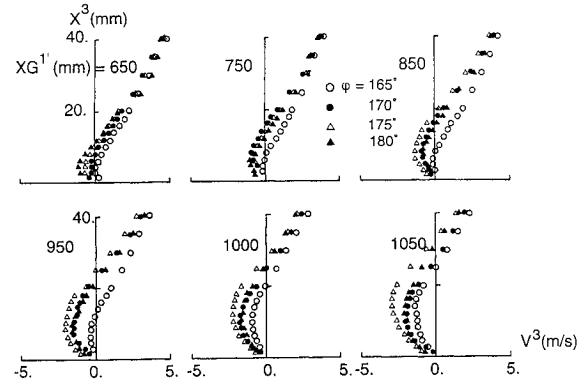

Fig. 13 Normal mean velocity component V^3. α = 20 deg, V_0 = 50 m/s, R_e = 5.6 × 10^6.

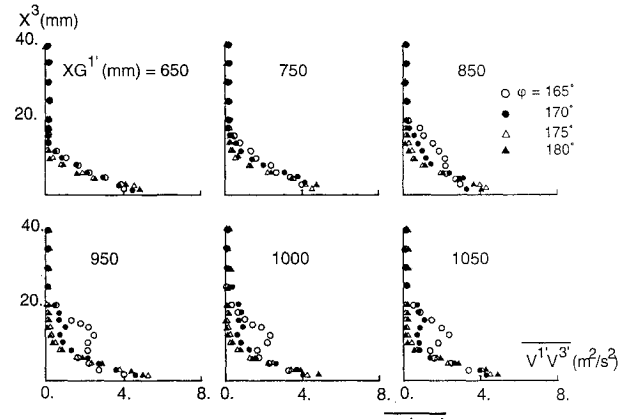

Fig. 14 Reynolds shear stress component $\overline{V^{1'}V^{3'}}$. α = 20 deg, V_0 = 50 m/s, R_e = 5.6 × 10^6.

to the plane of symmetry ($V^2 = 0$), which is the limit between the two preceding regions, moves from a position very close to the wall at $XG^{1'}$ = 650 mm to a greater height for the downstream sections.

As already indicated, the crosswise component V^2 is zero in the plane of symmetry, whereas its derivative ($\partial V^2/\partial X^2$) is different from zero (the derivative would be also zero for a purely two-dimensional flow).

The profiles of the normal mean velocity component V^3 are plotted in Fig. 13. They also exhibit two well-defined regions. In the outer region, V^3 is positive, and the flow direction is accordingly upwards. In the region near the wall, V^3 is negative, and the flow direction is downwards. For the first plane ($XG^{1'}$ = 650 mm), the inner part is very thin, the magnitude of the negative values of V^3 being small. For this section, we can consider the boundary-layer flow to be practically parallel to the wall. For the three following sections, and along the meridian line φ = 165 deg, V^3 is nearly equal to zero in the wall region. But for the three other meridian lines, an inner region with negative values of V^3 appears and grows in size. In the last two sections, the profiles in the different meridian lines all contain a region where V^3 takes on negative values. But for a given cross section ($XG^{1'}$ = constant plane), the height where $V^3 = 0$ differs for each meridian line, in contrast with the behavior observed for V^2.

Figure 14 shows the profiles of the turbulent shear stress $\overline{V^{1'}V^{3'}}$ for the six cross sections and the four values of the meridian angle φ. For φ = 170 and 165 deg from abscissa $XG^{1'}$ = 950 mm, a second extremum appears some distance from the surface of the model. The amplitude of this second extremum increases as we go downstream. From the oil flow visualization we observed that this extremum corresponded to development of the separation lines and therefore the vortex. The center of the vortex is situated on the meridian line φ = 165 deg at X^3 = 10 mm (see also Fig. 10 for section $XG^{1'}$ = 950 mm). The same observation can be made for the results relative to the shear stress component $\overline{V^{2'}V^{3'}}$ (see Fig. 15).

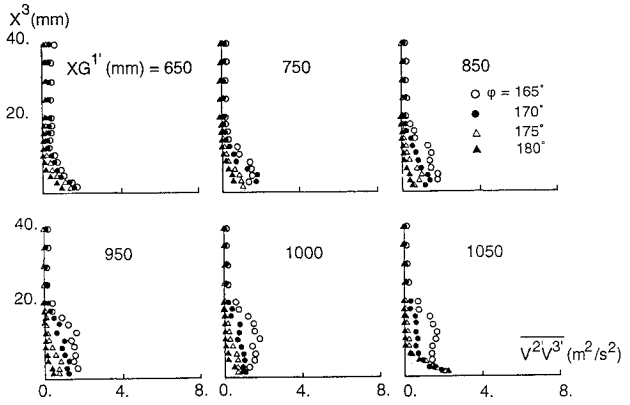

Fig. 15 Reynolds shear stress component $\overline{V^{2'}V^{3'}}$. α = 20 deg, V_0 = 50 m/s, $R_e = 5.6 \times 10^6$.

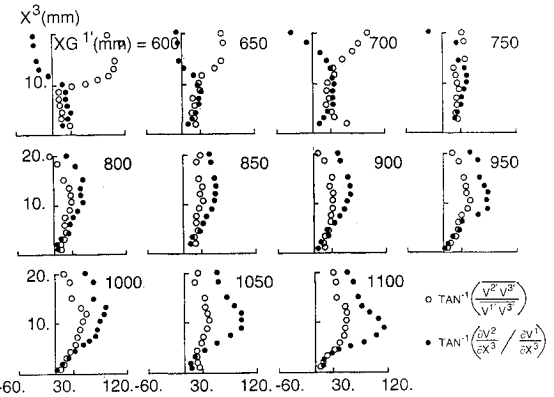

Fig. 16 Comparison between $\text{TAN}^{-1}(\overline{V^{2'}V^{3'}}/\overline{V^{1'}V^{3'}})$ and $\text{TAN}^{-1}((\partial V^2/\partial X^3)/(\partial V^1/\partial X^3))$. φ = 170 deg, α = 20 deg, V_0 = 50 m/s, $R_e = 5.6 \times 10^6$.

Figure 16 shows a comparison between the direction of the shear stress vector (components $\overline{V^{2'}V^{3'}}$ and $\overline{V^{1'}V^{3'}}$) and the direction of the mean velocity gradient vector (components $\partial V^1/\partial X^3$ and $\partial V^2/\partial X^3$). The results concern the meridian line φ = 170 deg. Down to section $XG^{1'}$ = 800 mm, the two vectors are nearly aligned (taking into consideration measurement uncertainties). Downstream of this section, and with the exception of a thin layer in contact with the wall, a difference in direction between the two vectors appears and increases with the downstream distance. For these experiments, the shear stress vector lags behind the velocity gradient vector. Similar behavior was observed by Bradshaw and Pontikos.[39]

It is clear that in this part of the flow a turbulence model based on an isotropic eddy viscosity model should not be used, since such an assumption implies that the shear stress and the mean velocity gradient vectors are aligned. This anisotropic effect must be taken into account in turbulence models, for example by using the adaptation proposed by Abid et al.[40]

External Flowfield Measurements with the Three-Component LDV System

At large circumferential angles from the plane of symmetry, the LDV system must be used in backscatter mode because of the obstruction caused by the model. Under these conditions, measurements close to the model wall are difficult because of the large amount of stray light emitted by the surface.

Because of these difficulties, it was decided to investigate only downstream cross planes, where the vortex is well detached from the wall. The first section thus considered was located at $XG^{1'}$ = 900 mm and coincided with the last section studied with the three-hole pressure probes. The last section, at $XG^{1'}$ = 1300 mm, contains a well-organized vortex flow.

Figure 17 shows the streamlines obtained from the mean velocity components V^2 and V^3 in planes normal to the model longitudinal axis. For the first section, V^3 is small and vortex development occurs

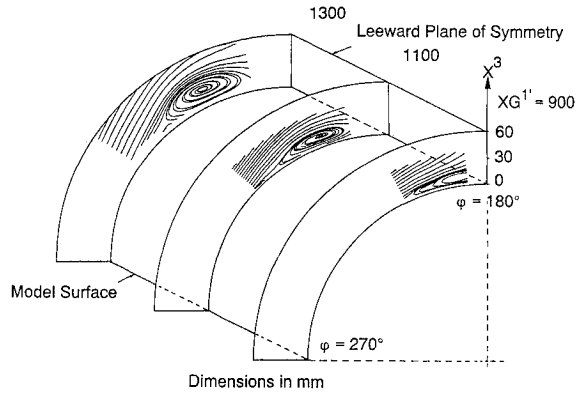

Fig. 17 Streamlines projections in the planes normal to the model longitudinal axis (from 3D LDV measurements). α = 20 deg, V_0 = 50 m/s, $R_e = 5.6 \times 10^6$.

near the leeward plane of symmetry and close to the wall. For the other two planes further downstream, the vortex moves away from the leeward plane of symmetry, and its core is at a greater distance from the model wall.

Conclusions

Mean velocity and turbulent shear stress measurements were made in the region of the leeward plane of symmetry of an ellipsoid cylinder set at incidence of 20 deg in a 50-m/s uniform flow.

Several means of investigation were used according to the region of the flow to be studied. The most accurate results are relative to the boundary layer in the leeward plane of symmetry. There, the flow was probed using a three-component LDV system operating in forward scatter mode. Information was obtained on both the mean and the fluctuating flow properties. However, in the forward scatter mode of operation, it was only possible to make measurements near the model surface in meridian planes close to the plane of symmetry. Thus, to study the flow in a more extended region, the LDV system was also used in backscatter mode. Unfortunately, in this configuration, the quality of the signal tends to become significantly degraded, especially in near-wall regions.

The description of the flowfield was completed by measurements made from 0.5 mm of the model surface using three-hole pressure probes. These measurements gave information on the boundary-layer behavior in the region of formation of the separation lines. However, this type of probe does not allow turbulence measurements.

Also, surface pressure measurements and surface flow visualizations were made. They showed that for a 20-deg incidence, separation had no appreciable effects on surface pressure.

The preceding series of tests allowed a detailed description of the flow in the region where separation giving rise to the formation of a vortical structure takes place. It was observed how the boundary layer gradually evolved from a shear flow confined in a thin layer in contact with the wall into a vortical structure formed by curling of the separated dissipative flow. At the same time, when skewing of the boundary layer induced by the separation process increased, the difference in direction between the velocity gradient and the shear stress vector also increased. It is clear that for this type of flow turbulence models should take these observations into account.

Acknowledgments

The authors are greatly indebted to the F2 Wind Tunnel Group of the ONERA Fauga-Mauzac test center for performing the experiments.

References

[1]Eichelbrenner, E. A., "Décollement Laminaire en Trois Dimensions sur un Obstacle Fini," ONERA, No. 89, Chatillon, France, Oct. 1957.

[2]Werlé, H., "Etude Expérimentale au Tunnel Hydrodynamique de l'Ecoulement Autour d'une Famille d'Ellipsoïdes aux Faibles Vitesses," ONERA, NT 1/1859 A, Chatillon, France, July 1957.

[3]Kreplin, H.-P., Meier, H. U., and Maier, A., "Wind Tunnel Model and Measuring Techniques for the Investigation of Three-Dimensional Turbulent Boundary Layers," *Proceedings of the AIAA 10th Aerodynamic Testing Conference* (San Diego, CA), AIAA, New York, 1978, pp. 93–97 (AIAA Paper 78-781).

[4]Kreplin, H.-P., Vollmers, H., and Meier, H. U., "Experimental Determination of Wall Shear Stress Vectors on an Inclined Prolate Spheroid," *Proceedings of the 5th US/FRG DEA Meeting*, Wright–Patterson AFB, OH, 1980, pp. 315–332 (AFFDL-TR-80-3088).

[5]Raynal, J. C., and Pelissier, C., "Essai dans la Soufflerie F1/CFM d'un Ellipsoïde de Révolution du DFVLR," ONERA, Procés Verbal d'Essais 1/7252 ANG, Chatillon, France, Feb. 1983.

[6]Kreplin, H.-P., Meier, H. U., and Vollmers, H., "Wall Shear Stress Measurements on a Prolate Spheroid at Zero Incidence in the ONERA F1 Wind Tunnel—Data Report," DFVLR, IB 222-84A35, Göttingen, Germany, Nov. 1984.

[7]Schneider, G. R., "Calculation of Three-Dimensional Boundary Layers on Bodies of Revolution at Incidence," *Proceedings of the 5th US/FRG DEA Meeting*, Wright–Patterson AFB, OH, 1980, pp. 287–314 (AFFDL-TR-80-3088).

[8]Cebeci, T., "Problems and Opportunities with Three-Dimensional Boundary Layers," AGARD Round Table Discussion on Three-Dimensional Boundary Layers, Invited Paper, Brussels, May 1984.

[9]Patel, V. C., and Baek, J. H., "Boundary Layers and Separation on a Spheroid at Incidence," *AIAA Journal*, Vol. 23, No. 1, 1985, pp. 55–63.

[10]Van Dalsem, W. R., and Steger, J. L., "The Efficient Simulation of Separated Three-Dimensional Viscous Flows Using the Boundary-Layer Equations," AIAA Paper 85-4064, Oct. 1985.

[11]Cebeci, T., and Meier, H. U., "Turbulent Boundary Layer on a Prolate Spheroid," AIAA Paper 87-1299, June 1987.

[12]Iyer, V., and Harris, J. E., "Solution of the Surface Euler Equations for Accurate Three-Dimensional Boundary-Layer Analysis of Aerodynamic Configurations," AIAA Paper 87-1154, June 1987.

[13]Wie, Y.-S., and Dejarnette, F. R., "Numerical Investigation of Three-Dimensional Flow Separation Using the Boundary Layer Equations," AIAA Paper 88-0617, Jan. 1988.

[14]Délery, J. M., and Formery, M. J., "A Finite Difference Method for Inverse Solutions of 3-D Turbulent Boundary Layer Flow," AIAA Paper 83-0301, Jan. 1983.

[15]Barberis, D., "A Direct-Inverse Finite Difference Method for 3-D Boundary-Layer Calculation Past Arbitrary Bodies," AIAA Paper 86-1827, June 1986; see also ONERA, TP 1986-57, Chatillon, France, 1986.

[16]Radwan, S. F., and Lekoudis, S. G., "Inverse Mode Calculations of the Incompressible Turbulent Boundary Layer on an Ellipsoid," *AIAA Journal*, Vol. 24, No. 10, 1986, pp. 1628–1635.

[17]Anon., AGARD Fluid Dynamics Panel, Working Group 10, "Calculation of 3D Separate Turbulent Flows in Boundary Layer Limit," AGARD, Advisory Rept. 255, NATO, May 1990.

[18]Rebuffet, P., "Maquette d'Ellipsoïde Aplati-Répartition de Pression, Etude de la Transition de la Couche Limite," ONERA, PV 5/1728 A, Chatillon, France, July 1957.

[19]Costis, C. E., "Separation and Wakes over Three-Dimensional Bodies," Ph.D. Thesis, Dept. of Engineering Science and Mechanics, Virginia Polytechnic Inst. and State Univ., Blacksburg, VA, 1985.

[20]Costis, C. E., Polen, D. M., Hoang, N. T., and Telionis, D. P., "Laminar Separating Flow Over a Prolate Spheroid," AIAA Paper 87-1212, June 1987.

[21]Barber, K. M., and Simpson, R. L., "Mean Velocity and Turbulence Measurements of Flow Around a 6:1 Prolate Spheroid," AIAA Paper 91-0255, Jan. 1991.

[22]Hsieh, T., "An Investigation of Surface Flow Pattern and Pressure Distribution for Viscous Sonic Flow over a Hemisphere-Cylinder at Incidence," *Proceedings of the IUTAM Symposium on 3D Turbulent Boundary Layers*, edited by H. H. Fernholz and E. Krause, Springer–Verlag, Berlin, Germany, 1982, pp. 243–253.

[23]Kordulla, W., Vollmers, H., and Dallmann, U., "Simulation of Three Dimensional Transonic Flow with Separation Past a Hemisphere-Cylinder Configuration," *Proceedings of the AGARD Symposium on Applications of Computational Fluid Dynamics in Aeronautics*, AGARD-CP-412, NATO (Aix-en-Provence, France), 1986, pp. 31.1–31.15.

[24]Hoang, N. T., and Telionis, D. T., "The Hemisphere-Cylinder at an Angle of Attack," AIAA Paper 90-0050, Jan. 1990.

[25]Ramaprian, B. R., Patel, V. C., and Choi, D. H., "Mean Flow Measurements in the Three-Dimensional Boundary Layer over a Body of Revolution at Incidence," *Journal of Fluid Mechanics*, Vol. 103, Feb. 1981, pp. 479–504.

[26]Wang, K. C., "Three-Dimensional Boundary Layer near the Plane of Symmetry of a Spheroid at Incidence," *Journal of Fluid Mechanics*, Vol. 43, Pt. 1, 1970, pp. 187–209.

[27]Schneider, G. R., and Zhu, Z., "The Calculation of Incompressible Three-Dimensional Laminar and Turbulent Boundary Layers in the Plane of Symmetry of a Prolate Spheroid at Incidence," DFVLR, FB-82-16, Göttingen, Germany, July 1982.

[28]Schneider, G. R., "Calculation of Three-Dimensional Boundary Layers in the Plane of Symmetry of a Prolate Spheroid at Incidence Including the Laminar-Turbulent Transition," *Proceedings of the 8th US/FRG DEA Meeting on Viscous and Interacting Flow Field Effects* (Göttingen, Germany), 1983, pp. 39–48.

[29]Barberis, D., "Boundary-Layer Computation on Arbitrary Obstacles with Direct and Inverse Methods," *La Recherche Aérospatiale* (English translation), No. 3, Dec. 1986, pp. 1–27.

[30]Patel, V. C., and Baek, J. H., "Boundary Layers in Planes of Symmetry, Part II: Calculations for Laminar and Turbulent Flows," *AIAA Journal*, Vol. 25, No. 6, 1987, pp. 812–818.

[31]Patel, V. C., and Baek, J. H., "Boundary Layers in Planes of Symmetry, Part I: Experiments in Turbulent Flow," *AIAA Journal*, Vol. 25, No. 4, 1987, pp. 550–559.

[32]Sohn, C. H., Choi, D. H., and Chung, M. K., "Calculation of Plane-of-Symmetry Boundary Layers with a Modified k-ε Model," *AIAA Journal*, Vol. 29, No. 3, 1991, pp. 395–400.

[33]Chanetz, B., "Contribution à l'Etude du Décollement Tridimensionnel en Ecoulement Turbulent Incompressible," Thèse de Doctorat, ONERA, NT-1988-6, Chatillon, France, Oct. 1988.

[34]Afchain, D., Broussaud, P., Frugier, M., and Rancarani, G., "La Soufflerie F2 du Centre du Fauga-Mauzac," *20e Colloque d'aérodynamique appliquée*, AAAF Toulouse, ONERA, (TP) 1983-139, Toulouse, France, Nov. 1983.

[35]Werlé, H., "Principaux types de Décollement Libre Observés sur Maquettes Ellipsoïdales," ONERA, NT-1985-7, Chatillon, France, Dec. 1985.

[36]Quélin, C., and Barberis, D., "Etalonnage et Utilisation des Sondes Anémoclinométriques 3 Trous," ONERA, RT 104/1865 AN, Chatillon, France, Feb. 1988.

[37]Quélin, C., "Mise en Service de la Soufflerie S19 Implantée dans le Hall du Bâtiment AY du Parc de Chalais-Meudon," ONERA, RT 134/1865 AN, Chatillon, France, July 1991.

[38]Chanetz, B., "Décollement Tridimensionnel sur un Ellipsoïde-Cylindre de Révolution, Résultats de la Première Campagne d'Essais à F2," ONERA, RT 16/7252 AN, Chatillon, France, Feb. 1986.

[39]Bradshaw, P., and Pontikos, N. S., "Measurements in the Turbulent Boundary Layer on an 'Infinite' Swept Wing," *Journal of Fluid Mechanics*, Vol. 159, Oct. 1985, pp. 105–130.

[40]Abid, R., Délery, J., and Schmitt, R., "An Examination of Turbulence Models for a Separating Three-Dimensional Turbulent Boundary Layer," *Symposium on Numerical Methods in Laminar and Turbulent Flows* (Swansea, Wales, UK), edited by C. Taylor, J. A. Johnson, and W. R. Smith, ONERA TP No. 1985-74, Chatillon, France, Pineridge Press, 1985.